International Journal Of
Industrial Electronics Control and Optimization
Print ISSN: 3517-2645
Online ISSN: 3568-2645
Homepage: https://ieco.usb.ac.ir/

A Compact, High Efficiency, and Portable Wireless EV Resonant Charger

Jasem Shahsevani | Reza Beiranvand
Tarbiat Modares University, Faculty of Electrical and Computer Engineering, Tehran, Iran
Corresponding Author's Email: beiranvand@modares.ac.ir

Article Info

Article type:
Research Article

Article history:
Received: 23-August-2024
Received in revised form: 03-October-2024
Accepted: 15-November-2024
Published online: 22-June-2025

Keywords:
AC/DC converter,
Charger,
EV charger,
Interleaved converter.

ABSTRACT

Efficient and versatile charging solutions are essential for modern applications requiring portable energy systems. This paper presents a novel portable charger powered by an isolated split-core current clamp, enabling direct charging from power lines. The system utilizes inductive coupling to draw AC current from these lines, which is then regulated to a precise voltage for battery replenishment. The proposed design features an interleaved resonant topology with a semi-active rectifier, achieving high efficiency and adaptability to a wide range of input voltages. This architecture supports a variable DC bus voltage, enabling the resonant converter to operate optimally near its resonant frequency for maximum performance. To ensure a lightweight and efficient design, the converter eliminates traditional transformers, incorporating a capacitive element within the resonant network for galvanic isolation. A cascaded dual-control strategy in the interleaved structure ensures precise voltage regulation. Designed to be compatible with 1-6 cell Li-Ion batteries, the charger offers extensive versatility. Experimental results from a 2.5-200 W prototype, with an output voltage range of 4.2-25.2 V, demonstrate a peak efficiency of 94%, validating the effectiveness of the proposed charger for grid-connected applications.

I. Introduction

Electric Vehicles (EVs) have become integral to modern technological landscapes, serving critical roles in fields such as logistics, precision agriculture, and emergency services [1, 2]. Despite these advancements, a primary challenge persists: limited operation range due to high power consumption and constrained battery capacity. While increasing battery capacity might appear as a straightforward solution, it invariably results in additional weight, which in turn undermines the overall operational efficiency and maneuverability of EVs. Various strategies have been explored to extend operation duration, including the use of Capacitive Coupling Wireless Power Transfer (CCWPT) for charging [3, 4]. These methods typically rely on static charging stations, positioned along predetermined operational paths, requiring the EV to pause at specific nodes for recharging. This disrupts continuous operation and is impractical in rural or remote regions, limiting the potential reach of such systems. Research on optimizing battery utilization and operational paths to enhance range efficiency has shown some promise [5, 6], but the fundamental issues remain unresolved. In the realm of wireless power transfer, Inductive Coupling Wireless Power Transfer (ICWPT) has been extensively investigated [7-21], with advancements such as dynamic charging stations and repositionable transmitter coils for enhanced alignment and power transfer efficiency [9-20], Despite these improvements, most ICWPT systems necessitate precise alignment between the EV and charging unit, making them suboptimal for real-time and in-operation applications.

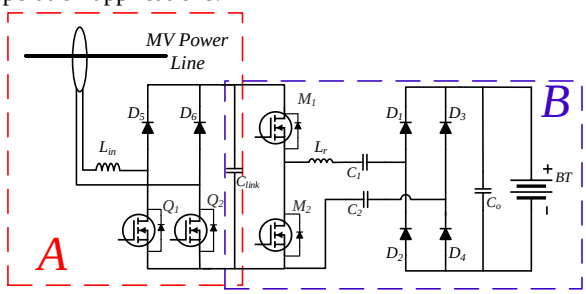


Fig. 1. The proposed portable EV charger.

Copyright © R. Beiranvand (s).
Publisher: University of Sistan and Baluchestan

TABLE1 LI-POL BATTERIES VOLTAGES FOR CHARGING

Number of Cells	Cut off Voltage	Nominal Voltage	Max. Voltage
1	3.0 V	3.7 V	4.2 V
2	6.0 V	7.4 V	8.4 V
3	9.0 V	11.1 V	12.6 V
4	12.0 V	14.8 V	16.8 V
5	15.0 V	18.5 V	21.0 V
6	18.0 V	22.2 V	25.2 V

A major limitation of existing EV charging systems is the low efficiency and power density of the converters employed. Most conventional solutions are heavily dependent on fixed charging infrastructure or constrained by optimization-based routing to maximize the operational radius. Consequently, these methods lack several critical attributes, such as a lightweight form factor, wide input/output voltage adaptability, high efficiency across varying voltage levels, and the capability for in-operation or contactless charging.

To address these limitations, various high-efficiency AC/DC and DC/DC converters have been proposed. While isolated AC/DC converters with transformers offer galvanic isolation, they suffer from increased size and weight, posing a significant drawback for EV applications [22, 23], Non-isolated AC/DC converters provide an alternative but lack the necessary isolation for safety and performance. Similarly, conventional DC/DC converters designed for battery charging are encumbered by bulky transformers, reducing their feasibility for compact EV systems [24, 25]. Non-isolated DC/DC converters have also been explored [26, 27], but they present challenges in terms of safety and electromagnetic interference (EMI) concerns. Furthermore, AC/DC converter designs developed for high-power grid applications [28, 29] are not well-suited for EV charging due to their substantial size, reliance on input inductors, and inability to function effectively with dynamic input voltages encountered during in-operation charging scenarios.

Additionally, existing solutions often lack adequate filtering mechanisms before the transformer stage, leading to increased harmonic distortion, reduced efficiency, and elevated thermal losses. Moreover, the limited input/output voltage range of conventional converters restricts their operational flexibility, failing to meet the diverse voltage requirements of different battery configurations [30-34], Although a few approaches have incorporated capacitive isolation to mitigate transformer-related drawbacks [35] they still fall short in achieving the desired combination of lightweight structure, broad voltage adaptability, and in-operation charging capability.

In this paper, we present a novel transformer-less isolated AC/DC resonant converter specifically designed for EV charging, with a focus on Lithium-Polymer (Li-Pol) batteries. To ensure a compact and portable solution, the proposed converter utilizes a transformer-less topology, employing two series capacitors for galvanic isolation and an interleaved resonant structure for enhanced efficiency. The converter integrates a circular split-core current clamp, enabling it to connect to power lines or perform in-operation charging by harnessing inductive coupling to generate AC voltage. A sophisticated dual-control mechanism is implemented within the interleaved structure, ensuring optimal performance and high efficiency over a wide range of input voltages and operational conditions. The proposed converter successfully addresses the aforementioned limitations, offering a robust solution for uninterrupted EV operation and extended performance range.

The remainder of the paper is structured as follows: Section II presents the proposed converter's architecture and key operating waveforms. Section III provides a detailed analysis of its operational states and control approach, followed by an in-depth analysis of losses in Section IV. Section V discusses the design procedure and validation through experimental results is debated in Section VI. Finally, Section VII concludes the paper by highlighting the significance and potential impact of the proposed converter in advancing EV charging technologies.

II. Proposed Converter and Its Key Waveforms

Lithium-Polymer (Li-Pol) batteries are widely utilized in EVs due to their high capacity and power output, making them suitable for applications that demand lightweight and high-energy density. These batteries typically operate within a voltage range of 4.2-25.2 V, depending on the configuration of one to six cells, with each cell having a maximum voltage of 4.2 V. However, EVs equipped with such batteries face limitations in operation duration, which typically ranges between 15 to 45 minutes, consequently restricting their operational range. To overcome this constraint, an advanced EV charging solution is proposed to enhance operation radius and continuity. The charger addresses critical design considerations such as lightweight structure, broad input/output voltage range, and high efficiency across varying voltage levels, compact form factor for easy installation, and in-operation charging capability. The proposed charging system, illustrated in Fig. 1, is designed to interface with power lines by either direct contact or proximity-based power transfer, allowing the EV to recharge while in motion. It features a split-core current clamp with an adjustable aperture, enabling the EV to connect seamlessly to the power line and induce AC voltage into the converter's input stage, for example as shown in Fig. 2. The converter’s input stage comprises an AC voltage source fed into a semi-active rectifier, which includes a small inductor. This rectifier converts the induced AC voltage into a variable DC voltage to accommodate fluctuations in the input supply and maintain stable output. Following the rectification stage, a series resonant converter is employed. This converter serves two essential functions: first, it stabilizes voltage fluctuations caused by the small input inductor, ensuring a smooth and regulated output voltage. Secondly, it provides input-output isolation through two series

capacitors integrated within the resonant structure, eliminating the need for a traditional transformer and thereby reducing weight and size. By adopting a resonant topology with interleaved operation and semi-active rectification, the proposed converter efficiently charges Li-Pol batteries from one to six cells. The resonant converter operates primarily near its resonant frequency in the ZVS region, enabling soft switching for high efficiency. To further optimize performance, a large link capacitor (C_{link}) is introduced to maintain a stable voltage. However, by allowing up to a 20% voltage variation in Clink, the size of both Clink and the input inductor (L_{in}) can be significantly reduced. This variation is managed by the closed-loop control implemented in Section B of the converter, minimizing the impact on output voltage regulation.

In summary, the variable input voltage governs the overall regulation of the output voltage, while the resonant converter provides galvanic isolation and contributes minimally to output regulation, ensuring high efficiency and lightweight design. Fig. 1 illustrates the architecture of the proposed converter, with Section A responsible for charging the C_{link} capacitor, and Section B regulating the output voltage and powering the load. Fig. 2 demonstrates an application of the converter, and Fig. 3 presents key operational waveforms, showcasing the performance and efficiency of the proposed system.

III. Different Operational States of the Converter and Its Control Algorithm

This section elaborates on the different operational states of the proposed converter and the corresponding control algorithm. The semi-active rectifier is controlled using a Phase-Shift Modulation (PSM) approach at a switching frequency of 300 kHz, while the resonant converter (Section B in Fig. 1) employs a Pulse Frequency Modulation (PFM) strategy within the same frequency range. Due to the significantly higher switching frequency compared to the grid frequency, the grid voltage can be approximated as a DC voltage source for the converter. The overall control scheme is a cascaded configuration, integrating PFM and PSM, wherein the semi-active rectifier primarily manages the output voltage regulation. To minimize the converter's size, a reduced-value input inductor and link capacitor are utilized, which results in a ripple on the link capacitor's voltage. The resonant stage, positioned downstream, mitigates these voltage fluctuations, providing a stable output voltage suitable for battery charging. This is achieved through a dual-loop cascade control approach: an inner PFM loop for the resonant stage and an outer, slower PSM loop for overall output voltage regulation.

The operational states of the isolated converter, which utilizes capacitors C_1 and C_2 for isolation, are depicted in Fig. 3 and are described as follows:

State I: During the interval t_0–t_1 (Fig. 3), switches Q_1 and Q_2 are both turned on, causing L_{in} to charge. As there is no power transfer to C_{link}, its voltage drops. Simultaneously, in Section B, M_1 is conducting, allowing power to flow through C_r, D_1, and D_4 to the load, as shown in Fig. 4(a).

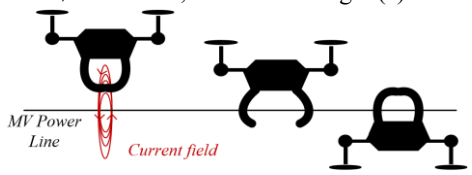


Fig. 2. An Application of the proposed converter for EV charging via in-operation charging through induced current fields or direct connection to power lines.

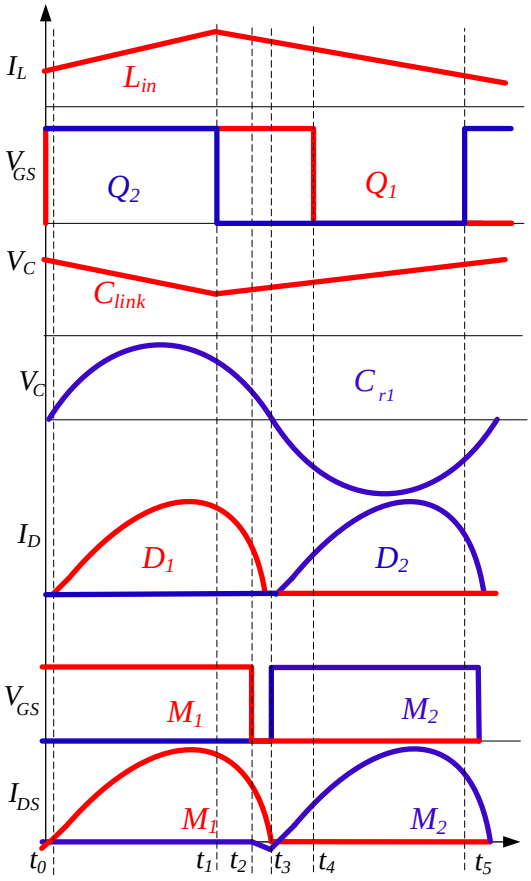


Fig. 3. Some of proposed converter key waveforms in 300 kHz switching frequency operation.

State II: In the interval t_1–t_2 , Q_2 is turned off, halting L_{in}'s charging. L_{in} then discharges into C_{link}, increasing its voltage.

Section B continues its previous operation, as shown in Fig. 4(b).

State III: During t_2–t_3, Section A maintains the previous operation. In Section B, at t_2, M_1 is turned off, and its current passes through M_2's body-diode, achieving Zero Voltage Switching (ZVS) for M_2's turn-on. This action turns off D_1 and D_4, as depicted in Fig. 4(c).

State IV: At t_3, Q_2 is turned off, leaving L_{in} and C_{link} operations unchanged. In Section B, M_2 is turned on under ZVS conditions, energizing D_2 and D_3, as shown in Fig. 4(c).

State V: At t_4, Q_2 is turned on again, and Section B continues its previous operation. Subsequently, the cycle repeats periodically, as illustrated in Fig. 4(d).

It is noteworthy that when Q_1 and Q_2 are turned off, their body-diodes conduct, causing Section A to function as a diode bridge. The converter's output voltage is regulated using a combination of PSM and PFM control. While PFM control tends to be less efficient under low-load conditions, the interleaved structure mitigates efficiency loss. To maintain high efficiency, Section B predominantly operates at the resonant frequency during typical operational conditions. The output voltage is further regulated by the PSM control in Section A, whereas Section B ensures isolation and closed-loop control of the output voltage, significantly influencing the size of the input inductor.

The frequency response characteristics of the proposed converter under various quality factors (Q) and phase shifts are shown in Fig. 5, illustrating its operational dynamics and efficiency performance.

IV. Mathematical Power Loss Analysis

Here, some important power loss components of the proposed converter are calculated. The equations (1-20) are mainly derived from [2, 36, 37].

A. Diode

$$i_{D1}(t)=\begin{cases} n\,I_{Rm}\sin(\omega_o t) & 0\le t<\frac{1}{2}T_o,\\ 0 & \frac{1}{2}T_o\le t<T_s. \end{cases} \quad (1)$$

$$i_{D2}(t)=\begin{cases} 0 & 0\le t<\frac{1}{2}T_s,\\ n\,I_{Rm}\sin(\omega_o t) & \frac{T_s}{2}\le t<\frac{T_s+T_0}{2},\\ 0 & \frac{T_s+T_0}{2}\le t<T_s. \end{cases} \quad (2)$$

Where, ω_o is equal to $2\pi f_o$. In result RMS and average current through each diodes is:

$$I_{D1_{avg}}=\frac{I_o}{2}, I_{Rm}=\frac{\pi I_o}{2n\frac{f_s}{f_o}},\quad I_{D1_{avg}}=\frac{\pi I_o}{4}\sqrt{\frac{f_o}{f_s}}. \quad (3)$$

So power loss due V_f of each diode is:

$$P_{Vf}=V_f I_{D1_{avg}}=V_f\frac{I_o}{2}=\frac{V_f}{V_o}\frac{P_o}{2}. \quad (4)$$

Therefore, we can write:

$$P_{rf}=I_{D1_{rms}}^2 r_f=\frac{\pi^2}{16}\frac{f_o}{f_s}\frac{r_f}{R_L}P_o. \quad (5)$$

$$P_D=P_{D1}+P_{D2}=\left(\frac{V_f}{V_o}+\frac{\pi^{16}}{8}\frac{f_o}{f_s}\frac{r_F}{R_L}\right)P_o. \quad (6)$$

A. Output Capacitor

Output capacitor current is:

$$I_{Co}(t)=\begin{cases} n\,I_{Rm}\sin(2\omega_o t)-I_o & 0\le t<\frac{T_0}{2},\\ -I_o & \frac{T_0}{2}\le t<T_s. \end{cases} \quad (7)$$

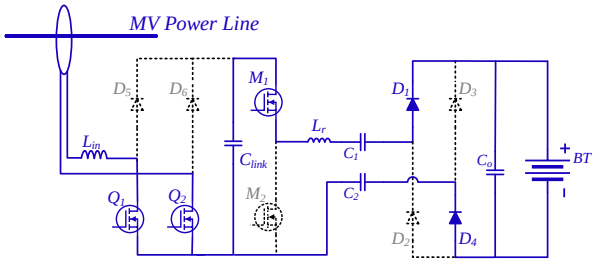
$$I_{Co_{rms}}=I_o\sqrt{\frac{\pi^2}{8}\frac{f_o}{f_s}-1}. \quad (8)$$

So its power loss is as follows:

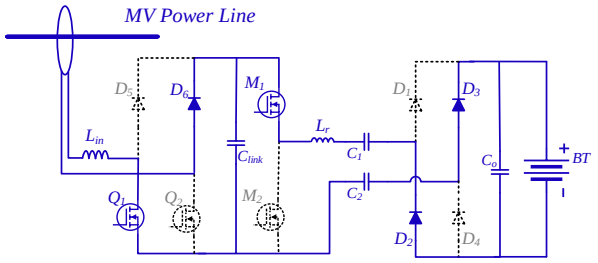
$$P_{r_{Co}}=I_{Co_{rms}}^2 r_{Co}=\left(\frac{\pi^2}{8}\frac{f_o}{f_s}-1\right)I_o^2 r_{Co}$$

$$=\left(\frac{\pi^2}{8}\frac{f_o}{f_s}-1\right)\frac{r_{Co}}{R_L}P_o. \quad (9)$$

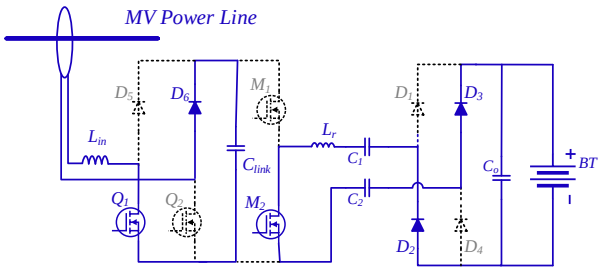
In addition, to calculate the power MOSFET switches losses, following parameters are given:



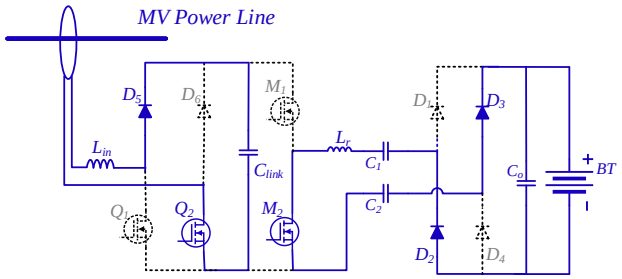
(a)



(b)



(c)



(d)

Fig. 4. The operation of proposed converter.

Discharge Time (t_{dis}): The time it takes for the DC capacitor to discharge from the input voltage to 0 V after the MOSFET is switched off.

Dead Time (t_{dead}): The time interval between the gate-source signals of the high-side and low-side MOSFETs in a half-bridge configuration. This prevents shoot-through current, which can damage the MOSFETs.

Turn-on Delay ($t_{delay(on)}$): The time it takes for the drain-source current to start flowing after the gate-source voltage reaches the threshold voltage.

Body Diode Conduction Time ($t_{body(on)}$): The time the internal body diode of the MOSFET conducts during the turn-on transition.

Gate-Source Voltage (V_{gs}): The voltage applied between the gate and source terminals of the MOSFET.

Body Diode Forward Voltage (V_{bF}): The voltage drop across the body diode when it conducts current.

MOSFET Conduction Time ($t_{ds(on)}$): The time the MOSFET conducts current during the switching cycle.

B. Power MOSFET Drive Circuit Power Loss

This kind of loss is due to gate-source power MOSFET capacitor charge and discharge, which is as follows:

$$P_{drive} = 2\left(\frac{1}{2}C_{gs}V_{gs}^2\right)f_s. \tag{10}$$

C. Diode and MOSFET Body Diode Power Losses

$$t_{dis} = \frac{8}{M_g}L_m(C_{ds1} + C_{ds2})f_s. \tag{11}$$

$$t_{body(on)} = t_{dead} - t_{dis} + t_{delay(on)}. \tag{12}$$

$$P_{body} = 2V_{bF}\left[\left(\frac{nV_o}{L_m}\left(\frac{1}{4}\frac{1}{f_s} - t_{dis}\right)\right)\right]t_{body(on)}f_s. \tag{13}$$

D. MOSFET Turning off Switching Loss

Two assumptions are made in this section. The first one is in the meanwhile of power MOSFET turning off, which its current is near the inductor magnetizing current, and the second one is rising voltage and magnetizing inductor current is linear.

$$V_{ds}(\mathrm{t}) = V_{ds(on)} + \frac{V_{in} - V_{ds(on)}}{t_{dis}}t. \tag{14}$$

$$i_{ds}(t) = \frac{nV_o}{L_m}\frac{1}{4f_s}\left(1 - \frac{t}{t_{dis}}\right). \tag{15}$$

$$p_{tf} = 2f_s\int_0^{t_{dis}} v_{ds}(t)i_{ds}(t)dt$$

$$= \frac{nV_o t_{dis}}{12L_m}\left(V_{in} + 2V_{ds(on)}\right). \tag{16}$$

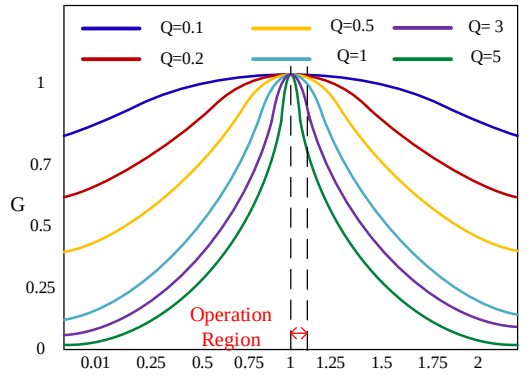
Some other parameters are given as follows:

$$F = \frac{f_s}{f_r}, \qquad f_r = \frac{1}{2\pi\sqrt{L_r C_{eq}}}, \quad \omega = \frac{1}{2\pi f_r}. \tag{17}$$

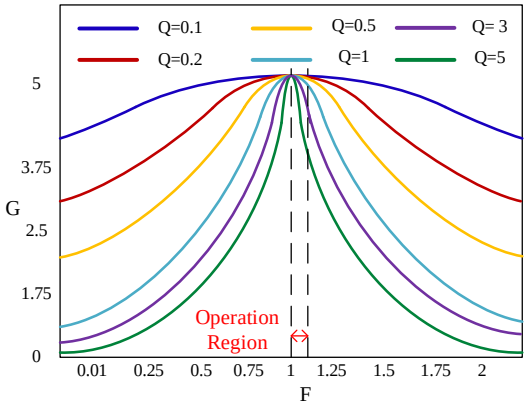
$$R_{eq} = \frac{8}{\pi^2}R_L, \quad Q = \frac{1}{R_{eq}}\sqrt{L_r/C_{eq}}. \tag{18}$$

$$i_{Q1,2(AVG)} = \frac{V_i DT}{2L}\frac{V_i D}{V_o - V_i} = \frac{0.02\,V_i^2 D^2}{2L(V_o - V_i)}. \tag{19}$$

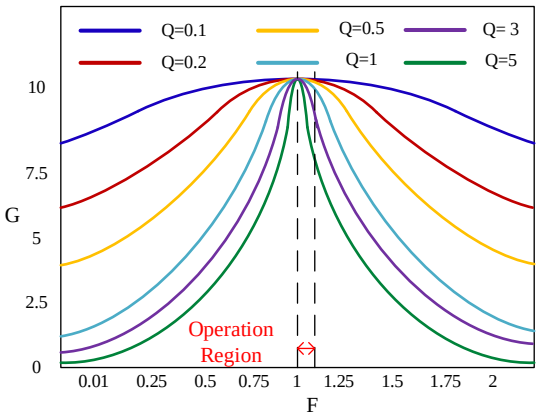
$$D = \frac{\theta_2 - \theta_1}{360} = 1 - \frac{V_{in}}{2V_{out}} \tag{20}$$



(a) Phase-shift= 180°.



(b) Phase-Shift= 90°.



(c) Phase-shift= 0 degree.

Fig. 5. Normalized gain-frequency characteristics of the proposed converter for different quality factors (Q) in (a) Phase-shift=180° (b) Phase-shift=90° (c) Phase-shift=0°.

V. Converter Design Procedure

The design of the proposed converter, specifically tailored for EV charging applications, prioritizes minimizing volume and weight. Typically, the input inductor (L_{in}) in such converters is large and cumbersome. To mitigate this issue, a 20% allowable voltage variation in the output of Section A (as depicted in Fig. 1) is considered. This variation is then corrected by the

- individual capacitor value

must be calculated accordingly.

The design procedure for the converter is visually summarized in Fig. 6.

C. Design of the Circular Current Clamp:

To ensure accurate and efficient power transfer, the design of the circular current clamp must follow these steps:

1. *Define Primary and Secondary Parameters:*
   - The current flowing through the MV power lines is sinusoidal at 50 Hz. Define the power line voltage and its maximum current (I_p). Determine the voltage required at the secondary side (V_s) to meet the charger's specifications.
2. *Selection of Ferrite Core:*
   - Choose a ferrite core suitable for the application. Based on the EV's size and weight limitations, define the core's physical parameters, including the length of the magnetic path (lll) and the cross-sectional area (A) in meters.
3. *Calculation of Number of Turns:*
   - Using Equation (23), calculate the number of turns required for the core, where μ is the permeability of the core material, and $\omega=2\pi f$ is the angular frequency of the grid voltage.

This structured approach ensures the proposed converter meets the stringent requirements for EV charging applications, including compactness, high efficiency, and compatibility with MV power lines.

feedback control loop in Section B. By accepting this voltage fluctuation, the size and volume of L_{in}can be significantly reduced. The design procedure is outlined in the following steps:

A. Design of Section A:

- *Input Inductor (L_{in}) and Link Capacitor (C_{link}):* Calculate the values of L_{in} and C_{link} using Equations (21) and (22). The duty cycle (D) of the semi-active rectifier can be derived using Equation (20). These components are selected to balance efficiency, size, and weight.

B. Design of Section B:

- *Equivalent Load Resistance (R_{eq}):* Determine R_{eq} using Equation (18). Based on the Gain-Frequency-Phase Shift characteristics, select a suitable curve that meets the desired design requirements, including voltage gain and the preferred range of switching frequencies.
- *Quality Factor (Q) and Resonant Frequency:* Identify the quality factor (Q) and the corresponding exact switching frequency from the chosen curve on the Gain-Frequency-Phase Shift characteristics.
- *Resonant Capacitors (C_r) and Inductor (L_r):* Determine C_r and L_r using Equations (17) and (18) as a system of two equations with two unknowns. Note that C_r represents the total capacitance for the two series capacitors, and each

$$L_{in} \leq \frac{D(1-D)V_{out}}{2\, f_s I_{L_r}} \tag{21}$$

$$C_{link} \leq \frac{D\, I_{out_max}}{0.2\, f_s V_{out}} \tag{22}$$

$$N = \frac{V_s\, l}{\omega\, \mu\, A\, I_p} = \sqrt{\frac{\omega\, \mu\, A\, I_p^2}{P_s\, l}} \tag{23}$$

VI. Experimental Results

To validate the performance of the proposed charger, an experimental prototype was developed to charge 1 to 6 cell Li-Polymer (Li-Pol) batteries, with a power range of 2.5–220 W. For the prototype system, a current clamp, similar to the design depicted in Fig. 7(b), was used to feed the converter. In an industrialized version, the current clamp will be redesigned for a more compact structure and integrated into the converter's control system. The specifications of the prototype converter are listed in Table 2, and the prototype is shown in Fig. 7(a), with its input sourced from the AC current clamp.

The performance of the charger was evaluated under two worst-case scenarios: (i) lowest output power at the highest input voltage and (ii) highest output power at the lowest input voltage. The experimental results for Section B under these conditions are presented in Fig. 8, while Figs. 9 and 10 show the results for Section A. The efficiency curve of the charger is illustrated in Fig. 11.

In both test cases, Section B of the converter operates close to its resonant frequency, ensuring high efficiency. Section A, operating in a broader voltage range, provides the suitable output voltage, though with a notable ripple on C_{link}. Section B then smooths this ripple, providing a stable, regulated output voltage and electrical isolation for the batteries. The proximity to the resonant frequency minimizes noise and enhances efficiency, resulting in similar operational waveforms for both worst-case conditions.

The experimental results demonstrate that the proposed charger meets the stringent requirements of Li-Pol battery charging for EV applications. The charger exhibits robust performance in terms of voltage regulation, power transfer efficiency, and other key metrics, confirming its suitability for EV charging applications. To further emphasize the advantages of the proposed design, a comparison with conventional converters is provided in Table 3, highlighting the superior features and efficiency of the proposed charger.

The charger supports both connected and wireless charging modes, offering flexibility in various operational scenarios.

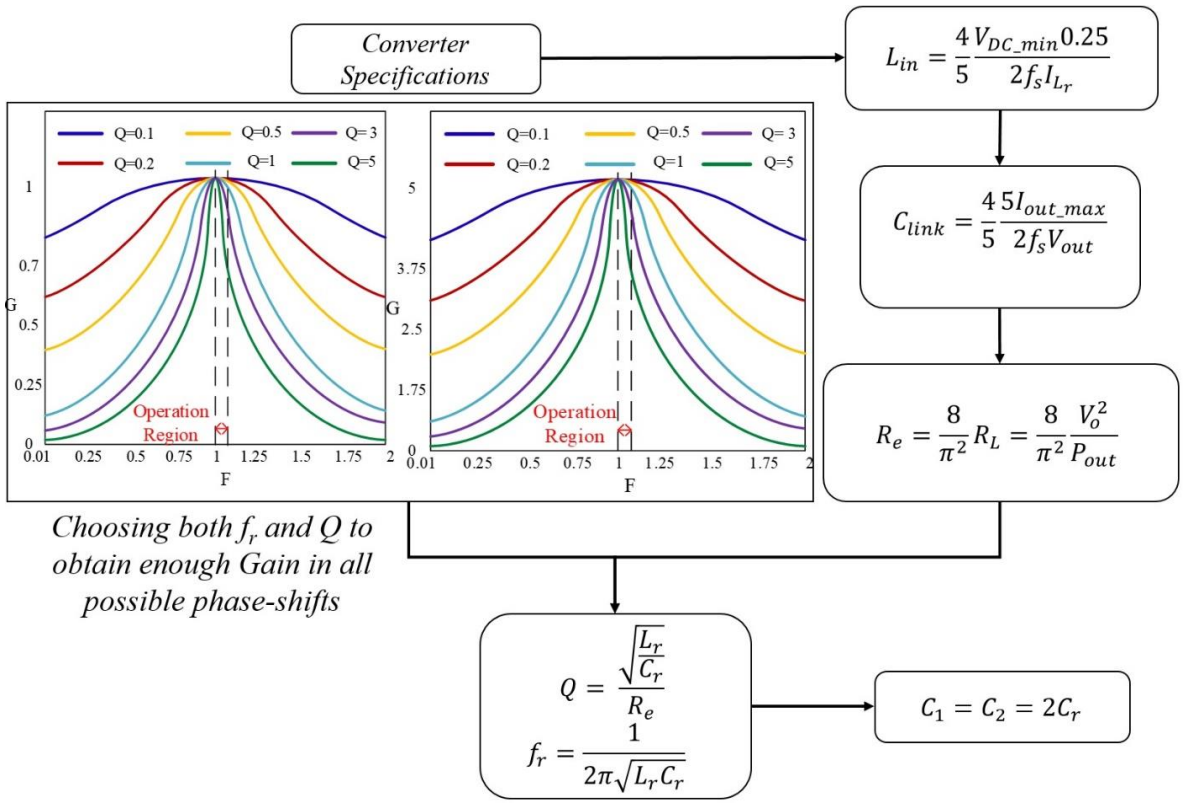


Fig. 6. Design procedure of the proposed converter.

A. *Connected Charging Mode:* In this mode, the process begins by opening the current clamp. Upon engagement with the power line, the clamp induces power that is subsequently transferred to the EV's batteries via the integrated DC-DC converter system this ensures efficient power transfer, effectively charging the batteries and optimizing their performance and lifespan.

B. *Wireless Charging Mode:* In this mode, the current clamp remains closed as the EV flies over the power lines. The innovative design of the clamp allows the current field generated by the power lines to pass through, inducing power within the clamp. The sophisticated converter system then adjusts the output voltage as necessary, ensuring optimal charging conditions tailored to the EV's battery specifications.

The seamless transition between connected and wireless charging modes enhances the charger's adaptability to diverse charging scenarios, maximizing its efficiency and utility. By incorporating dual-mode functionality, the proposed charger offers unparalleled flexibility, whether in connected mode (where power is harnessed directly from the grid) or in wireless mode (where power is induced as the EV flies over power lines). This innovative approach streamlines the charging process and significantly enhances overall operational efficiency and productivity.

VII. Conclusion

This paper presents a novel high-efficiency charger designed specifically to address the limitations of conventional EV charging systems. The proposed charger stands out due to several critical features tailored to the unique requirements of EV applications. EVs, which are characterized by limited payload capacities, require lightweight charging systems to avoid compromising their operational performance. To achieve a compact design, the traditional transformer-based structure has been eliminated, significantly reducing the size

and weight of the converter. Despite the exclusion of the transformer, which typically provides isolation and voltage ratio control, the proposed converter effectively overcomes these challenges through a strategic combination of design elements.

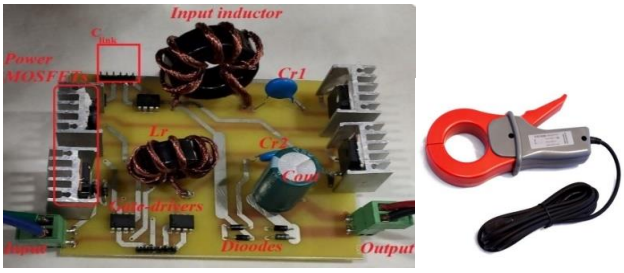
First, isolation is ensured by incorporating two capacitors within the converter's resonant structure, providing the necessary electrical separation between the input and output. Second, the adoption of a semi-active rectifier at the input stage allows for precise AC voltage regulation and enables the desired voltage ratio control, compensating for the lack of a traditional transformer. Moreover, the converter is designed with a minimized input inductor and link capacitor to achieve a lightweight and compact configuration. Although this introduces voltage ripple at the output, a cascade control approach—comprising an outer Phase-Shift Modulation (PSM) loop for the semi-active rectifier and an inner, faster Pulse-Frequency Modulation (PFM) loop for the resonant converter—ensures a well-regulated output voltage suitable for battery charging.

Another key advantage of the proposed converter is its ability to operate with high efficiency over a wide range of input and output voltages. By using the semi-active rectifier as the primary voltage provider, the resonant section of the converter can function near its resonant frequency, resulting in several benefits. This design approach not only maximizes efficiency—critical for portable chargers where energy loss can significantly impact performance—but also minimizes thermal losses that could otherwise lead to overheating and adversely affect the EV's operation. Moreover, operating near the resonant frequency reduces electromagnetic interference, ensuring stable and reliable performance under varying load conditions.

In summary, the proposed charger offers a unique combination of features, including a lightweight and compact structure, a broad input and output voltage range, high efficiency, and low noise operation, making it a versatile and robust solution for portable EV charging applications.

The current clamp used in conjunction with the converter allows the charger to connect directly to power lines, facilitating in-operation charging of Li-Pol batteries. The charger's innovative design also supports wireless charging by flying over MV power lines, where the current clamp induces power to charge the batteries during operation, thereby extending the EV's operational range. The charging process utilizes a circular split-core current clamp to extract power from the lines, with the induced AC voltage directed to the transformer-less semi-active resonant converter for efficient power transfer. The converter is capable of charging 1-6 cell Li-Pol batteries, demonstrating its versatility and adaptability for various EV battery configurations.

Experimental results validate the performance of the proposed converter, with the prototype system achieving a peak efficiency of 94% while charging batteries ranging from 2.5 W to 220 W. These results confirm the charger's high efficiency and suitability for both connected and wireless charging modes, underscoring its potential for broad application in EV missions requiring extended operation durations. With its compact design, high efficiency, and flexible charging capabilities, the proposed charger represents a significant advancement in EV power systems, addressing the limitations of existing solutions and setting a new benchmark for portable EV charging technology.



(a) (b)

Fig. 7. (a) Prototype converter, (b) current clamp, to be connected to power lines, the output of the current clamp is connected to the converter.

TABLE 2 THE PROTOTYPE CONVERTER SPECIFICATIONS

Parameter	Value
L_{in}	80 µH
L_r	10 µH
C_{r1}, C_{r2}	60 nF
C_{link}	1 mF
C_o	100 µF
Switching Frequency	290-310 kHz
CT Model	Current Clamp Adapter AC, 52 mm, 1000 A
Phase Shift	0-179 degree
Semi-Active Rectifier Switching Frequency	300 kHz
Output Voltage	Each cell maximum voltage according to Table I
Input Voltage	MV power line
Diode	MUR840
Switch	23N60E
Gate-Drive	TC4427

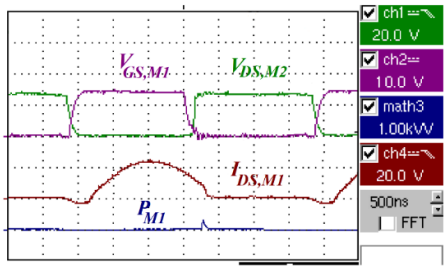
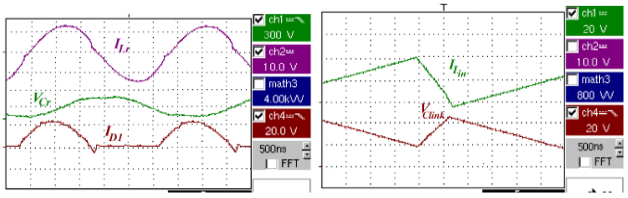


Fig. 8. M_1 and M_2 gate-source voltages, M_1 drain-source current, and M_1 power-loss experimental waveforms, respectively.



(a) (b)

Fig. 9. (a) Resonant inductor current, resonant capacitor voltage, and D_1 current waveforms and (b) input inductor current and C_{link} voltage in highest input voltage and lowest output power.

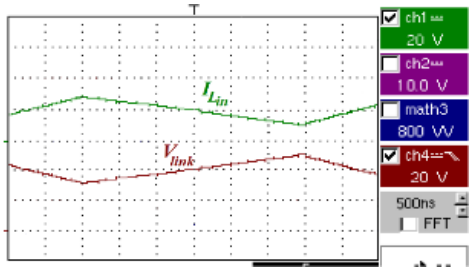


Fig. 10. Input inductor current and C_{link} voltage in lowest input voltage and highest output power.

TABLE 3 COMPARISON OF THE PROPOSED CONVERTER WITH SOME CONVENTIONAL CONVERTERS

	Reference	Input Voltage (V)	Output Voltage (V)	Output Power (W)	Peak-Efficiency (%)	Switching Frequency (kHz)	C_{bus} (µF)	L_{in} (µH)	L_r (µH)	C_r (nF)	Input/output Isolation Method	L_m (µH)	Converter and its control complexity	Number of Components
AC / DC	[34]	230 ac	400	2650	92.7	NM⸸	NO†	100 ×1000	206× 1000	NO	NO	NO	Medium	Medium
	[33]	160-220 ac	48	450	94.5	20	C_f= 0.47	L_f = 2300	NO	NO	NO	L_2= 40	Low	Medium
	[32]	160-260 ac	24 - 72	650	94	20	C_1= 0.47	L_i= 3500	NO	NO	TR*	NM	Low	Medium
	[31]	40-80 RMS	15-48	400	92	100	Cbus	NM	0.44	4.7	TR	NM	Low	Medium
PFC	[38]	85-265 ac	48	300	93	NM	120	NM	177	13	TR	NM	Low	Medium
	[39]	100-130 ac	48	350	92	140	400	2×110	70	16.4	TR	120	Low	Medium
	[40]	277-380 RMS ac	50	100	91	NM	440	NM	58	47	TR	275	High	High
	[29]	370-410	48	650	96	150-450	NM	NM	2×8	35	TR	105	Medium	Medium
WPT	[41]	200	200	1	90	~250	NO	NO	16.2	25	CWPT	81× 1000	Low	Low
	[42]	360-400	12	750	97	NM	NO	NO	19	64	IWPT	64	Medium	Low
	[43]	25-100	210	250	98	80-140	NO	NO	48	15 &5	IWPT	15.8 &5.4 9	Medium	Low
	[44]	390	60-450	NM	97	140	NO	NO	12.8	354	IWPT	354	Medium	Low
	[13]	24	15	30<	74	1000	NO	100	NO	100	IWPT	37	Low	Low
Proposed Converter		20 kV	4.2-25.2	220	94	290-310 kHz	1000	80	10	2×60	IWPT	NO	Medium	Medium

*** TR = Transformer**

† NO = There is no component in the structure

⸸NM = Not Mentioned

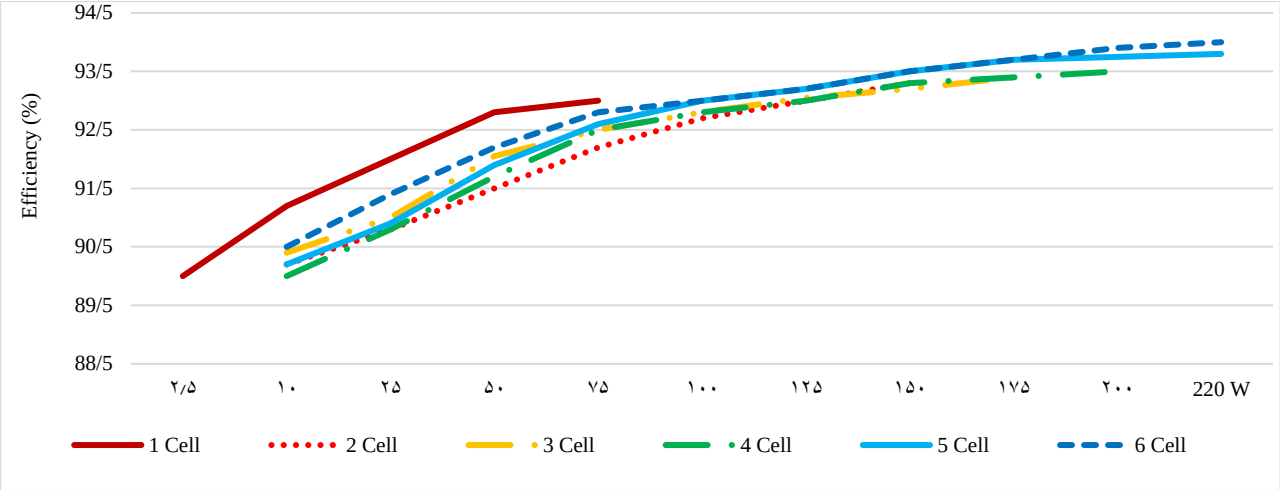


Fig. 11. Efficiency curves of the proposed converter for different types of batteries.

References

[1] J. Shahmoradi, E. Talebi, P. Roghanchi, and M. Hassanalian, "A comprehensive review of applications of EV technology in the mining industry," *EVs*, vol. 4, no. 3, p. 34, 2020.

[2] J. Shahsevani and R. Beiranvand, "An Application-Oriented Review of the LLC-Based Resonant Converters," *IEEE Access*, 2024.

[3] A. Muharam, T. M. Mostafa, and R. Hattori, "Design of power receiving side in wireless charging system for UAV application," in *2017 International Conference on Sustainable Energy Engineering and Application (ICSEEA)*, 2017: IEEE, pp. 133-139.

[4] D. Vincent, P. S. Huynh, L. Patnaik, and S. S. Williamson, "Prospects of capacitive wireless power transfer (C-WPT) for unmanned aerial vehicles," in *2018 IEEE PELS Workshop on Emerging Technologies: Wireless Power Transfer (Wow)*, 2018: IEEE, pp. 1-5.

[5] K. I. Kilic and L. Mostarda, "Heuristic EV pathfinding over optimized charging station grid," *IEEE Access*, vol. 9, pp. 164070-164089, 2021.

[6] H. Huang and A. V. Savkin, "Deployment of charging stations for EV delivery assisted by public transportation vehicles," *IEEE Transactions on Intelligent Transportation Systems*, 2021.

[7] C. H. Choi, H. J. Jang, S. G. Lim, H. C. Lim, S. H. Cho, and I. Gaponov, "Automatic wireless EV charging station creating essential environment for continuous EV operation," in *2016 International Conference on Control, Automation and Information Sciences (ICCAIS)*, 2016: IEEE, pp. 132-136.

[8] T. Campi, S. Cruciani, M. Feliziani, and F. Maradei, "High efficiency and lightweight wireless charging system for EV batteries," in *2017 AEIT International Annual Conference*, 2017: IEEE, pp. 1-6.

[9] J. Chen, C. W. Yu, and W. Ouyang, "Efficient wireless charging pad deployment in wireless rechargeable sensor networks," *IEEE Access*, vol. 8, pp. 39056-39077, 2020.

[10] A. M. Jawad, H. M. Jawad, R. Nordin, S. K. Gharghan, N. F. Abdullah, and M. J. Abu-Alshaeer, "Wireless power transfer with magnetic resonator coupling and sleep/active strategy for a EV charging station in smart agriculture," *IEEE Access*, vol. 7, pp. 139839-139851, 2019.

[11] T. Campi, S. Cruciani, F. Maradei, and M. Feliziani, "Innovative design of EV landing gear used as a receiving coil in wireless charging application," *Energies*, vol. 12, no. 18, p. 3483, 2019.

[12] A. Rohan, M. Rabah, M. Talha, and S.-H. Kim, "Development of intelligent EV battery charging system based on wireless power transmission using hill climbing algorithm," *Applied System Innovation*, vol. 1, no. 4, p. 44, 2018.

[13] A. M. Jawad *et al.*, "Wireless EV charging station using class-E power amplifier in vertical alignment and lateral misalignment conditions," *Energies*, vol. 15, no. 4, p. 1298, 2022.

[14] A. Carloni, F. Baronti, R. Di Rienzo, R. Roncella, and R. Saletti, "On the Sizing of the DC-Link Capacitor to Increase the Power Transfer in a Series-Series Inductive Resonant Wireless Charging Station," *Energies*, vol. 14, no. 3, p. 743, 2021.

[15] A. Rohan, M. Rabah, F. Asghar, M. Talha, and S.-H. Kim, "Advanced EV battery charging system," *Journal of Electrical Engineering & Technology*, vol. 14, no. 3, pp. 1395-1405, 2019.

[16] J. Zhou, B. Zhang, W. Xiao, D. Qiu, and Y. Chen, "Nonlinear parity-time-symmetric model for constant efficiency wireless power transfer: Application to a EV-in-operation wireless charging platform," *Ieee transactions on industrial electronics*, vol. 66, no. 5, pp. 4097-4107, 2018.

[17] D. Raveendhra, M. Mahdi, R. Hakim, R. Dhaouadi, S. Mukhopadhyay, and N. Qaddoumi, "Wireless charging of an autonomous EV," in *2020 6th International Conference on Electric Power and Energy Conversion Systems (EPECS)*, 2020: IEEE, pp. 7-12.

[18] K. Sang-Won, C. In-Kui, and H. Sung-Yong, "Comparison of charging region differences according to receiver structure in EV wireless charging system," in *2017 International Conference on Information and Communication Technology Convergence (ICTC)*, 2017: IEEE, pp. 1058-1060.

[19] S. W. Kim, I. K. Cho, and S. Y. Hong, "Design of transmitting coil for wireless charging system to expand charging area for EV applications," *Microwave and Optical*

Technology Letters, vol. 60, no. 5, pp. 1179-1183, 2018.

[20] C. Cai, J. Wang, H. Nie, P. Zhang, Z. Lin, and Y.-G. Zhou, "Effective-configuration WPT systems for EVs charging area extension featuring quasi-uniform magnetic coupling," *IEEE Transactions on Transportation Electrification*, vol. 6, no. 3, pp. 920-934, 2020.

[21] A. Raciti, S. A. Rizzo, and G. Susinni, "EV charging stations over the buildings based on a wireless power transfer system," in *2018 IEEE/IAS 54th Industrial and Commercial Power Systems Technical Conference (I&CPS)*, 2018: IEEE, pp. 1-6.

[22] R. Wu, S. B. Dewan, and G. R. Slemon, "A PWM AC-to-DC converter with fixed switching frequency," *IEEE Transactions on Industry Applications*, vol. 26, no. 5, pp. 880-885, 1990.

[23] P. N. Enjeti and S. A. Choudhury, "A new control strategy to improve the performance of a PWM AC to DC converter under unbalanced operating conditions," *IEEE Transactions on Power Electronics*, vol. 8, no. 4, pp. 493-500, 1993.

[24] S. Cuk, "A new zero-ripple switching DC-to-DC converter and integrated magnetics," *IEEE Transactions on Magnetics*, vol. 19, no. 2, pp. 57-75, 1983.

[25] B. Arnet and L. P. Haines, "High power DC-to-DC converter for supercapacitors," in *IEMDC 2001. IEEE International Electric Machines and Drives Conference (Cat. No. 01EX485)*, 2001: IEEE, pp. 985-990.

[26] S. Kim and F.-S. Kang, "Multifunctional onboard battery charger for plug-in electric vehicles," *IEEE Transactions on Industrial Electronics*, vol. 62, no. 6, pp. 3460-3472, 2014.

[27] F. Musavi, M. Craciun, D. S. Gautam, W. Eberle, and W. G. Dunford, "An LLC resonant DC–DC converter for wide output voltage range battery charging applications," *IEEE Transactions on Power Electronics*, vol. 28, no. 12, pp. 5437-5445, 2013.

[28] N. Bagheri, H. Alipour, L. Mohammadian, J. Beiza, and M. Ebadpour, "A Multiport isolated resonant LLC converter for grid-tied renewable energy powered bidirectional EV charger," *International Journal of Industrial Electronics Control and Optimization*, vol. 6, no. 1, pp. 37-48, 2023.

[29] E. L. Carvalho, A. Blinov, P. Emiliani, A. Chub, and D. Vinnikov, "Three-phase bidirectional isolated AC–DC matrix-converter with full soft-switching range," *IEEE Access*, vol. 11, pp. 119270-119283, 2023.

[30] I. Burgardt, C. B. Nascimento, A. A. Badin, and R. Gules, "An Integrated AC-DC Isolated Converter Electrolytic-Free with Intrinsic Active Low-Frequency Ripple Reduction," *IEEE Access*, 2024.

[31] Y. Y. Zandabad and S. S. Fazel, "A single-stage variable output AC-DC converter with PFC and soft-switching for renewable energy integration," *Energy Reports*, vol. 11, pp. 4873-4885, 2024.

[32] A. Singh, J. Gupta, and B. Singh, "Design and control of two stage battery charger for low voltage electric vehicles using high gain buck-boost PFC AC-DC converter," *IEEE Transactions on Industry Applications*, vol. 59, no. 5, pp. 6125-6135, 2023.

[33] A. D. Kumar, J. Gupta, and B. Singh, "A single-stage charger for lev based on quadratic buck-boost AC-DC converter topology," *IEEE Transactions on Industry Applications*, vol. 59, no. 4, pp. 4252-4263, 2023.

[34] V. Ramya and R. Marimuthu, "Integration of AC/DC With Multi Input Mode Selection Converter for Fast Charging of Battery in Electric Vehicles," *IEEE Access*, 2024.

[35] J. Shahsevani and R. Beiranvand, "A Bidirectional Resonant Converter for Capacitive Power Transmission in Electric Vehicle and PowerWall Applications," in *2023 31st International Conference on Electrical Engineering (ICEE)*, 2023: IEEE, pp. 264-270.

[36] V. Suel and S. Kizir, "A Comprehensive Loss Analysis of Half-Bridge LLC Resonant Converter used in LED Street Lights," in *2019 1st Global Power, Energy and Communication Conference (GPECOM)*, 2019: IEEE, pp. 146-151.

[37] C.-H. Yang, T.-J. Liang, K.-H. Chen, J.-S. Li, and J.-S. Lee, "Loss analysis of half-bridge LLC resonant converter," in *2013 1st International Future Energy Electronics Conference (IFEEC)*, 2013: IEEE, pp. 155-160.

[38] J. Yi, H. Ma, X. Li, S. Lu, and J. Xu, "A Novel Hybrid PFM/IAPWM Control Strategy and Optimal Design for Single-Stage Interleaved Boost-LLC AC–DC Converter With Quasi-Constant Bus Voltage," *IEEE Transactions on Industrial Electronics*, vol. 68, no. 9, pp. 8116-8127, 2020.

[39] R. Saasaa, W. Eberle, and M. Agamy, "A single-stage interleaved LLC PFC converter," in *2016 IEEE Energy Conversion Congress and Exposition (ECCE)*, 2016: IEEE, pp. 1-6.

[40] Z. Lu and L. Wei-Ming, "A Single-Stage LED Driver Using Step-Down Cuk/LLC with APWM-PFM Hybird Control," in *2018 15th China International Forum on Solid State Lighting: International Forum on Wide Bandgap Semiconductors China (SSLChina: IFWS)*, 2018: IEEE, pp. 1-4.

[41] D. Rozario, N. A. Azeez, and S. S. Williamson, "A modified resonant converter for wireless capacitive power transfer systems used in battery charging applications," 2016, Art no. 7520272, doi: 10.1109/ITEC.2016.7520272.

[42] E. Rong, S. Li, R. Zhang, X. Du, Q. Min, and S. Lu, "A magnetic integration half-turn planar transformer for LLC resonant DC-DC converters," in *2018 IEEE Applied Power Electronics Conference and Exposition (APEC)*, 2018: IEEE, pp. 484-488.

[43] H. Hu, X. Fang, F. Chen, Z. J. Shen, and I. Batarseh, "A modified high-efficiency LLC converter with two transformers for wide input-voltage range applications," *IEEE Transactions on Power Electronics*, vol. 28, no. 4, pp. 1946-1960, 2013, doi: 10.1109/TPEL.2012.2201959.

[44] D. Shu and H. Wang, "An Ultrawide Output Range ${LLC} $ Resonant Converter Based on Adjustable Turns Ratio Transformer and Reconfigurable Bridge," *IEEE Transactions on Industrial Electronics*, vol. 68, no. 8, pp. 7115-7124, 2020.



Jasem Shahsevani received his M.Sc. degree in power electronics engineering from Tarbiat Modares University, Tehran, Iran, in 2021. His current research interests include DC/DC converter, LLC-based resonant converter, wireless power transfer, electric vehicle charging, soft-switching techniques, and PV-based renewable energy systems.



Reza Beiranvand (Senior Member, IEEE) received the MSc and PhD degrees in electrical engineering from Sharif University of Technology, Tehran, Iran, in 1999 and 2010, respectively. From 2010 to 2012, he was a Postdoctoral research fellow with the Electrical Engineering College, Sharif University of Technology. From 1999 to 2007, he was an engineer at the R&D centers of PARS-Electric and RADIO SHAHAB MFGs, Tehran, Iran, where he was engaged in designing the LCD, and LED TVs based on the ST, LT, NXP, and Fairchild devices.

He is currently Head of the Power Electrical Engineering Department and Associate Professor with the Faculty of Electrical and Computer Engineering, Tarbiat Modares University, Tehran, Iran. His research interests include power electronics converters, soft switching techniques, SCCs, SMPS, Capacitive-Coupling Power Transfer and Inductive Power Transfer techniques, and PV-based renewable energy systems. Dr. Beiranvand was the IEEE Consultant (2017-2019) and Head of the Power Electrical Engineering Department (2018-2020) with the Tarbiat Modares University. He is between the top 2 % scientists of the world, based on the Stanford University; Stanford, CA, USA released lists, 2020-2024